Supporting Information

for

Manganese(II) Molecular Sources for Plasma-Assisted CVD of Mn Oxides and Fluorides: From Precursors to Growth Process

Davide Barreca,[‡] Giorgio Carraro,[†] Ettore Fois,[§] Alberto Gasparotto,[†] Filippo Gri,[†] Roberta Seraglia,[‡] Martin Wilken,[#] Alfonso Venzo,[‡] Anjana Devi, [#] Gloria Tabacchi[§] and Chiara Maccato[†]***

[‡] CNR-ICMATE and INSTM, Department of Chemical Sciences, Padova University, 35131 Padova, Italy.

[†] Department of Chemical Sciences, Padova University and INSTM, 35131 Padova, Italy.

[§] Department of Science and High Technology, University of Insubria and INSTM, 22100 Como, Italy.

[#] Inorganic Materials Chemistry, Faculty of Chemistry and Biochemistry, Ruhr-University Bochum, 44801 Bochum, Germany.

Computational Section

Density functional theory (DFT) calculations for geometry optimizations (GO) were performed on the $Mn(hfa)_2$•TMEDA and $Mn(tfa)_2$•TMEDA complexes by using the PBE functional[1] augmented with Hirao long-range corrections.[2-4] Calculations were carried out with the Gaussian 09 (G09) code.[5] The Stuttgart-Dresden ECP pseudopotentials were used with basis sets of the Stuttgart-Dresden type for all atoms.[6] The basis sets for H, C, N, O, and F atoms were augmented with diffuse and polarization functions taken from the (D95++(d,p)) basis set,[7] already used for other $M(hfa)_2$•TMEDA compounds (M= Fe, Co, Cu, Zn).[8-13] For both complexes, GO were performed by considering the following spin multiplicities: sextet, quartet, doublet. The highest-multiplicity spin state –namely, the sextet– was always energetically favored over the quartet and the doublet states by very large energy differences. Specifically, the calculated energy differences ΔE between sextet and doublet were 41.9 $kcal \times mol^{-1}$, for $Mn(hfa)_2$•TMEDA, and 44.1 $kcal \times mol^{-1}$, for $Mn(tfa)_2$•TMEDA, whereas the ΔE between sextet and quartet were 35.6 $kcal \times mol^{-1}$, for $Mn(hfa)_2$•TMEDA, and and 39.7 $kcal \times mol^{-1}$, for $Mn(tfa)_2$•TMEDA. Therefore, the spin state of $Mn(dik)_2$•TMEDA was defined to be a sextet and all other calculations on the neutral complexes were performed in this multiplicity.

All optimized structures resulted to be energy minima (with all positive frequencies). Optimized geometries and vibrational frequencies were also calculated for the three possible isomers of $Mn(tfa)_2$•TMEDA –iso1, iso2, iso3– shown in Figure 1. Relevant geometrical parameters of $Mn(hfa)_2$•TMEDA and of the three $Mn(tfa)_2$•TMEDA isomers are reported in Table S1, while calculated IR spectra for iso1, iso2, iso3 are shown in Figure S1. A constant shift factor of 0.963 was applied to the calculated vibrational frequencies in all reported simulated spectra.

The molecular ions $[Mn(dik)_2$•$TMEDA]^{+\bullet}$ were obtained by removing an electron from the $Mn(dik)_2$•TMEDA compounds and performing GO with the above-described computational approach and the same combination of DFT functionals/basis sets used for the neutral complexes. For both molecular ions, GO were performed by considering the following spin multiplicities:

quintet, triplet, singlet, and the lowest-energy spin state was found to be a quintet in view of the calculated energy differences. Specifically, the ΔE between quintet and singlet were: 48.4 kcal×mol^{-1} ([Mn(hfa)$_2$•TMEDA]$^{+\bullet}$); 56.7 kcal×mol^{-1} ([Mn(tfa)$_2$•TMEDA]$^{+\bullet}$), while the ΔE between quintet and triplet resulted: 9.6 kcal×mol^{-1} ([Mn(hfa)$_2$•TMEDA]$^{+\bullet}$) and 8.2 kcal×mol^{-1} ([Mn(tfa)$_2$•TMEDA]$^{+\bullet}$). All optimized structures were found to be energy minima, with positive frequencies. Relevant geometrical parameters are reported in Table S4.

The first principles molecular dynamics simulations (FPMD)[14] of the two parent Mn(dik)$_2$•TMEDA compounds were performed with the CPMD code[15] using the PBE approximation to DFT[1] with dispersion corrections,[16] plane wave (PW) basis sets, and ultrasoft pseudopotentials[17] for all atoms. Periodic boundary conditions were adopted, using a cubic box of 2.0 nm length. The adopted PW cut-off was 25 and 200 Ry for wavefunction and electronic density representation, respectively.

The FPMD simulations were started from the minimum structures of Mn(dik)$_2$•TMEDA obtained via GO. After equilibration, the room temperature behaviour of the two Mn(dik)$_2$•TMEDA complexes (sextet spin state) was followed by 10 ps-long simulations in the canonical NVT ensemble using T = 25°C as a target temperature and Nose-Hoover chain thermostats.[18-19] A time step of 0.121 fs was used for trajectory integration, with an inertia parameter of 500 atomic units (au) for the electronic coefficients.[20] In addition, since such a FPMD approach could adequately describe complex phenomena, even at non-standard conditions,[21] for a broad variety of organic-inorganic systems,[22-23] including also transition metals/metal cations,[24-26] we adopted it to explore the high-temperature dynamic behaviour of [Mn(dik)$_2$•TMEDA]$^{+\bullet}$ molecular ions.

For both systems, the 10-ps long FPMD simulations were performed, always in the canonical ensemble, using a target ionic temperature of 180°C. Moreover, in view of the relatively modest energy difference ΔE (triplet – quintet) calculated for these radical cations, two 10-ps long FPMD simulations were also performed for the two [Mn(dik)$_2$•TMEDA]$^{+\bullet}$ molecular ions in the triplet spin state. Relevant average geometrical parameters are reported in Table S5.

In all cases, 5-10 ps-long equilibration runs were performed prior to the production FPMD simulations.

Table S1. Calculated geometrical parameters of $Mn(dik)_2$•TMEDA [Hdik = 1,1,1,5,5,5-hexafluoro-2,4-pentanedione (Hhfa), or 1,1,1-trifluoro-2,4-pentanedione (Htfa)]. For Hdik=Htfa, the three possible isomers (iso1, iso2, iso3) were considered. Atom labeling: Oe1, Oe2 = equatorial oxygens; Oa1, Oa2 = axial oxygens (see also Figure 1).

distance (Å)	**hfa**	**iso1**	**iso2**[a]	**iso3**[b]
Mn–Oa1	2.123	2.117	2.137	2.106
Mn–Oa2	2.123	2.117	2.125	2.122
Mn–Oe1	2.128	2.120	2.110	2.144
Mn–Oe2	2.128	2.120	2.109	2.116
Mn–N1	2.248	2.303	2.232	2.257
Mn–N2	2.248	2.303	2.247	2.238
angle (º)				
Oa1–Mn–Oa2	171.5	177.3	166.7	170.5
Oe1–Mn–Oe2	86.6	100.4	87.3	85.3
N1–Mn–N2	81.4	79.5	81.5	81.2
Oa1–Mn–Oe2	81.9	82.7	95.4	96.5
Oa1–Mn–N2	96.2	86.4	97.8	87.1
Oa1–Mn–N1	90.3	91.5	91.4	91.9
N1-N2-Oe2-Oe1 dihedral angle (º)				
	−13.5	−13.6	10.4	7.2

[a]$\Delta E(iso2\text{-}iso1) = 2.9$ kcal×mol^{-1}; [b]$\Delta E(iso3\text{-}iso1) = 2.4$ kcal×mol^{-1}.

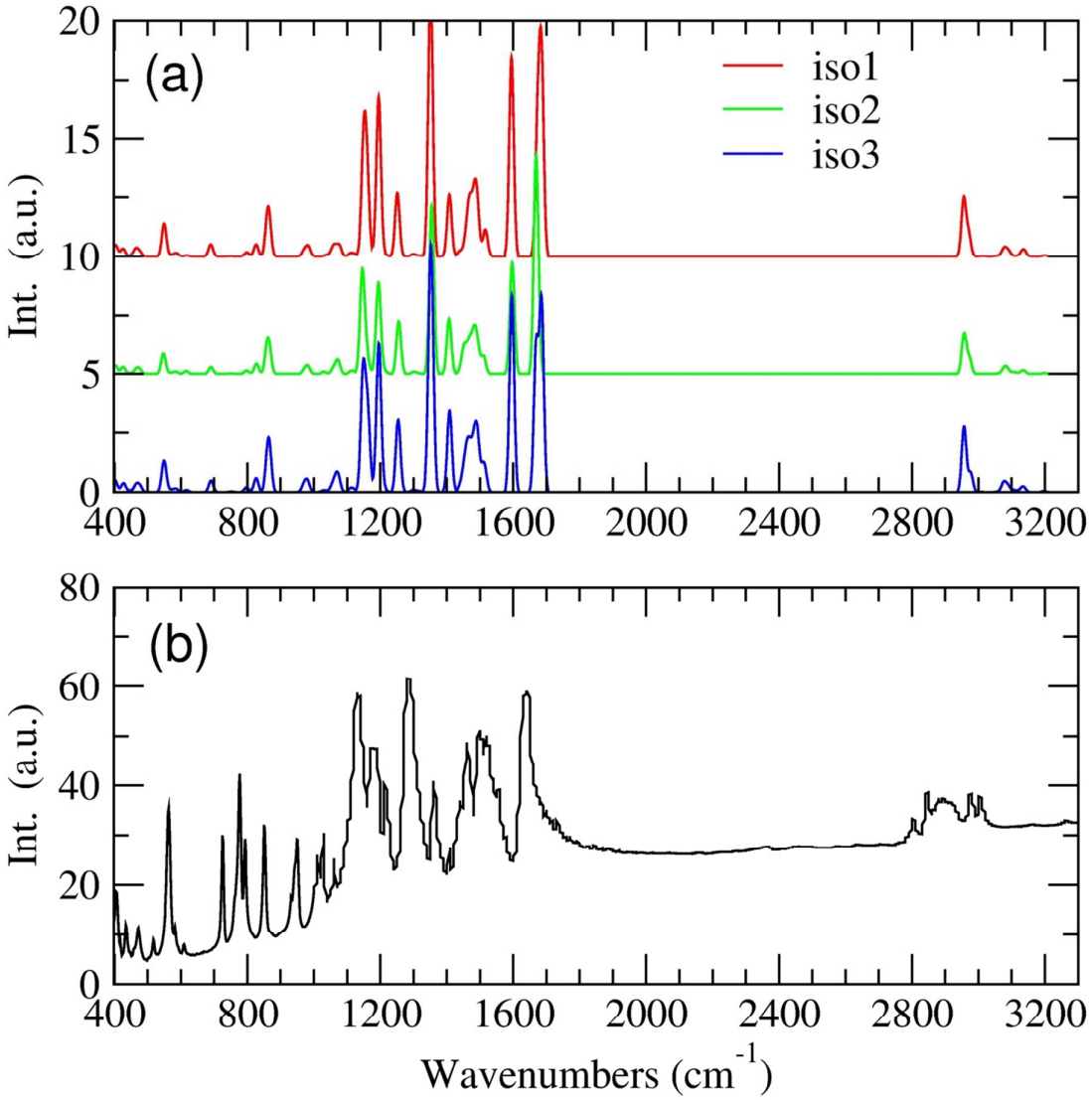

Figure S1. (a) Calculated IR spectra for the three isomers iso1, iso2, and iso3, of $Mn(tfa)_2$•TMEDA. (b) Experimental IR spectrum for the same compound (black line).

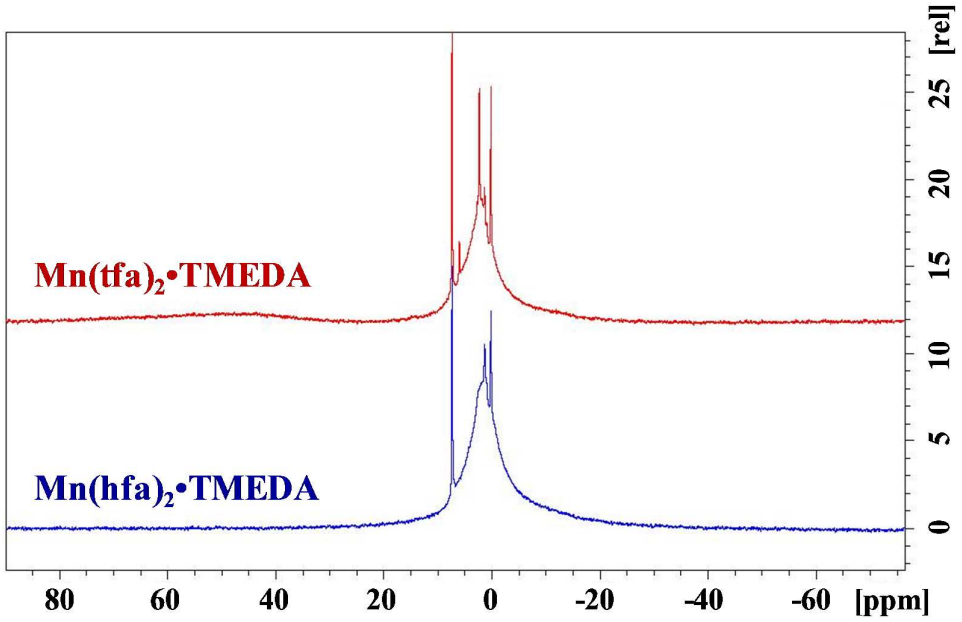

Figure S2. ^{1}H-NMR spectra of $Mn(hfa)_2$•TMEDA (bottom trace) and $Mn(tfa)_2$•TMEDA (top trace) (25°C; solvent, $CDCl_3$; ν_o = 200.13 MHz).

Table S2. Assignments of vibrational bands in the IR spectrum for **M**n(dik)$_2$•TMEDA complexes (dik = hfa, tfa).[a]

Vibrational mode	ν(Mn(hfa)$_2$•TMEDA) (cm^{-1})	ν(Mn(tfa)$_2$•TMEDA) (cm^{-1})
C-H stretching of dik ligands	3144	3162
C-H stretching of TMEDA ligand	3030-2780	3023-2790
C=O stretching of dik	1656	1640
Combinations of: C=C stretching of dik, C–H bending modes of dik, and CH_2/CH_3 deformation modes of TMEDA	1570-1435	1555-1420
C=C and CF_3 stretching modes	1346	
Bending CH_3 (scissoring)		1360
Combinations of: C–H bending and C–CF_3/CF_3 stretching modes	1110-1290	1120-1300
Combinations of C–C and C–N stretching modes	950-1100	930-1100
Out-of-plane bending of the C–H in dik	795	850
Vibrations of Mn–ligand bonds	400-527	400-560
Mn–O stretching	527	560
Mn–N stretching	473	468

[a] The assignment was made by the analysis of the normal modes obtained by the frequency calculation. Experimental IR bands are normally combinations of different modes. For the sake of clarity, only the main components of each IR band have been reported in the table.

Table S3. Peak positions (*m*/*z*) and pertaining relative abundances (R.A.%) in the EI-MS spectra of $Mn(dik)_2$•TMEDA compounds.

Ionic species	**$Mn(hfa)_2$•TMEDA** *m*/*z* **(R.A.%)**	**$Mn(tfa)_2$•TMEDA** **m/z (R.A.%)**
$[Mn(dik)_2•TMEDA]^{+•}$	585(0)	477 (0)
$[Mn(dik)_2]^{+•}$	469(2.1)	361 (42)
$[Mn(dik)_2–CF_3]^{+}$	400(3.1)	292 (33.2)
$[Mn(dik)•TMEDA]^{+}$	378(74.3)	324 (3.7)
$[Mn(dik)]^{+}$	262(1.8)	208 (28.1)
$[Mn(dik)–CF_2]^{+•}$	212(6.9)	158 (63.3)
$[TMEDA]^{+•}$	116(12.5)	116 (2.6)
$[(CH_3)_2N=CH_2]^{+}$	58(100)	58 (100)
CF_3^{+}	--	69 (9.3)

Table S4. Coordination bond lengths (Å) from GO of the $[Mn(dik)_2•TMEDA]^{+•}$ radical cations in the quintet, triplet, and singlet spin states.

	$[Mn(hfa)_2•TMEDA]^{+•}$			**$[Mn(tfa)_2•TMEDA]^{+•}$**		
Spin[a]	quintet	triplet	singlet	quintet	triplet	singlet
Bond[b]						
Mn-N1	2.036	2.021	2.029	2.099	2.034	2.029
Mn-N2	2.036	2.021	2.029	**2.253**	2.034	2.029
Mn-Oa1	**2.116**	1.866	1.863	1.852	1.854	1.833
Mn-Oa2	**2.116**	1.866	1.863	1.846	1.854	1.834
Mn-Oe1	1.889	1.906	1.887	1.949	1.912	1.942
Mn-Oe2	1.889	1.906	1.887	2.101	1.912	1.942

[a] The lowest-energy spin state is the quintet (see Computational Section). [b] Values highlighted in red-bold refer to the longest metal-ligand coordination distance.

Comment to Table S4. To facilitate comparison among the different spin states, this Table also contains the geometrical parameters of the minimum energy structures (quintet state) reported in Table 2 in the main text. In general, the geometry of the radical cations change appreciably with spin multiplicity. For this reason, and because of the modest energy difference between the optimized geometries of quintet and triplet (9.6 $kcal \times mol^{-1}$ ($[Mn(hfa)_2•TMEDA]^{+•}$) and 8.2 $kcal \times mol^{-1}$ ($[Mn(tfa)_2•TMEDA]^{+•}$), see also Computational section), FPMD simulations of the two radical cations were performed in the quintet and in the triplet state (cfr. Table S5).

Table S5. Average coordination bond lengths <r>±Δr[a] (Å) from the FPMD simulations of the $[Mn(dik)_2•TMEDA]^{+•}$ radical cations at 180°C in the quintet and triplet spin states.

	$[Mn(hfa)_2•TMEDA]^{+•}$		**$[Mn(tfa)_2•TMEDA]^{+•}$**	
spin[b]	quintet	triplet	quintet	triplet
Bond[c]				
Mn-N1	2.14 ±0.04	2.17±0.09	**2.25±0.10**	2.21 ±0.09
Mn-N2	2.14 ±0.04	2.17±0.10	**2.25±0.11**	2.19±0.11
Mn-Oa1	**2.16±0.08**	1.91 ±0.07	1.97±0.14	1.92±0.09
Mn-Oa2	**2.16±0.09**	1.91±0.08	1.99 ±0.12	1.92±0.10
Mn-Oe1	1.95 ±0.06	1.95 ±0.08	2.05±0.12	1.94 ±0.09
Mn-Oe2	1.95±0.07	1.94 ±0.07	2.05±0.12	1.94±0.09

[a] Δr provides an estimation of the amplitude of temperature-induced oscillations of metal-ligand bond distances. [b] The lowest-energy spin state is the quintet (see Computational Section). [c] Values highlighted in red-bold refer to the longest metal-ligand coordination distance.

Comment to Table S5. To facilitate comparison among the different spin states, this Table also contains the average geometrical parameters calculated from the FPMD of the two radical cations in the quintet state, reported in Table 2 in the main text.

References

(1) Perdew, J. P.; Burke, K.; Ernzerhof, M. Generalized Gradient Approximation Made Simple. *Phys. Rev. Lett.* **1996**, *77*, 3865-3868.

(2) Iikura, H.; Tsuneda, T.; Yanai, T.; Hirao, K. A Long-Range Correction Scheme for Generalized-Gradient-Approximation Exchange Functionals. *J. Chem. Phys.* **2001**, *115*, 3540-3544.

(3) Song, J.-W.; Hirosawa, T.; Tsuneda, T.; Hirao, K. Long-Range Corrected Density Functional Calculations of Chemical Reactions: Redetermination of Parameter. *J. Chem. Phys.* **2007**, *126*, 154105.

(4) Lange, A. W.; Rohrdanz, M. A.; Herbert, J. M. Charge-Transfer Excited States in a π-Stacked Adenine Dimer, As Predicted Using Long-Range-Corrected Time-Dependent Density Functional Theory. *J. Phys. Chem. B* **2008**, *112*, 6304-6308.

(5) Frisch, M. J.; Trucks, G. W.; Schlegel, H. B.; Scuseria, G. E.; Robb, M. A.; Cheeseman, J. R.; Montgomery Jr., J. A.; Vreven, T.; Kudin, K. N.; Burant, J. C.; Millam, J. M.; Iyengar, S. S.; Tomasi, J.; Barone, V.; Mennucci, B.; Cossi, M.; Scalmani, G.; Rega, N.; Petersson, G. A.; Nakatsuji, H.; Hada, M.; Ehara, M.; Toyota, K.; Fukuda, R.; Hasegawa, J.; Ishida, M.; Nakajima, T.; Honda, Y.; O. Kitao, N., H.; Klene, M.; Li, X.; Knox, J. E.; Hratchian, H. P.; Cross, J. B.; Bakken, V.; Adamo, C.; Jaramillo, J.; Gomperts, R.; Stratmann, R. E.; Yazyev, O.; Austin, A. J.; Cammi, R.; Pomelli, C.; Ochterski, J.; Ayala, P. Y.; Morokuma, K.; Voth, G. A.; Salvador, P.; Dannenberg, J. J.; Zakrzewski, V. G.; Dapprich, S.; Daniels, A. D.; Strain, M. C.; Farkas, O.; Malick, D. K.; Rabuck, A. D.; Raghavachari, K.; Foresman, J. B.; Ortiz, J. V.; Cui, Q.; Baboul, A. G.; Clifford, S.; Cioslowski, J.; Stefanov, B. B.; Liu, G.; Liashenko, A.; Piskorz, P.; Komaromi, I.; Martin, R. L.; Fox, D. J.; Keith, T.; Al-Laham, M. A.; Peng, C. Y.; Nanayakkara, A.; Challacombe, M.; Gill, P. M. W.;

Johnson, B. G.; Chen, W.; Wong, M. W.; C., G.; Pople, J. A., GAUSSIAN 09 (Revision D.02), Gaussian, Inc., Wallingford, CT. 2009.

(6) Bergner, A.; Dolg, M.; Küchle, W.; Stoll, H.; Preuß, H. Ab Initio Energy-Adjusted Pseudopotentials for Elements of Groups 13–17. *Mol. Phys.* **1993**, *80*, 1431-1441.

(7) Dunning Jr., T. H.; Hay, P. J., In *Modern Theoretical Chemistry*, Schaefer, H. F., Ed. Plenum: New York, 1976; Vol. 3.

(8) Bandoli, G.; Barreca, D.; Gasparotto, A.; Seraglia, R.; Tondello, E.; Devi, A.; Fischer, R. A.; Winter, M.; Fois, E.; Gamba, A.; Tabacchi, G. An Integrated Experimental and Theoretical Investigation on $Cu(hfa)_2TMEDA$: Structure, Bonding and Reactivity. *Phys. Chem. Chem. Phys.* **2009**, *11*, 5998-6007.

(9) Barreca, D.; Carraro, G.; Devi, A.; Fois, E.; Gasparotto, A.; Seraglia, R.; Maccato, C.; Sada, C.; Tabacchi, G.; Tondello, E.; Venzo, A.; Winter, M. β-Fe_2O_3 Nanomaterials from an Iron(II) Diketonate-Diamine Complex: a Study from Molecular Precursor to Growth Process. *Dalton Trans.* **2012**, *41*, 149-155.

(10) Barreca, D.; Carraro, G.; Gasparotto, A.; Maccato, C.; Seraglia, R.; Tabacchi, G. An iron(II) Diamine Diketonate Molecular Complex: Synthesis, Characterization and Application in the CVD of Fe_2O_3 Thin Films. *Inorg. Chim. Acta* **2012**, *380*, 161-166.

(11) Tabacchi, G.; Fois, E.; Barreca, D.; Gasparotto, A. CVD Precursors for Transition Metal Oxide Nanostructures: Molecular Properties, Surface Behavior and Temperature Effects. *Phys. Status Solidi A* **2014**, *211*, 251-259.

(12) Barreca, D.; Fois, E.; Gasparotto, A.; Seraglia, R.; Tondello, E.; Tabacchi, G. How Does CuII Convert into CuI? An Unexpected Ring-Mediated Single-Electron Reduction. *Chem. Eur. J.* **2011**, *17*, 10864-10870.

(13) Tabacchi, G.; Fois, E.; Barreca, D.; Gasparotto, A. Opening the Pandora's jar of Molecule-to-Material Conversion in Chemical Vapor Deposition: Insights from Theory. *Int. J. Quantum Chem.* **2014**, *114*, 1-7.

(14) Car, R.; Parrinello, M. Unified Approach for Molecular Dynamics and Density-Functional Theory. *Phys. Rev. Lett.* **1985**, *55*, 2471-2474.

(15) CPMD code, MPI für Festkörperforschung, Stuttgart, Germany; IBM Zürich Research Laboratory, Zürich, Switzerland, 1990–2017, www.cpmd.org.

(16) Grimme, S. Semiempirical GGA-type Density Functional Constructed with a Long-Range Dispersion Correction. *J. Comput. Chem.* **2006**, *27*, 1787-1799.

(17) Vanderbilt, D. Soft Self-Consistent Pseudopotentials in a Generalized Eigenvalue Formalism. *Phys. Rev. B* **1990**, *41*, 7892-7895.

(18) Nosé, S. A Unified Formulation of the Constant Temperature Molecular Dynamics Methods. *J. Chem. Phys.* **1984**, *81*, 511-519.

(19) Hoover, W. G. Canonical Dynamics: Equilibrium Phase-Space Distributions. *Phys. Rev. A* **1985**, *31*, 1695-1697.

(20) Blöchl, P. E.; Parrinello, M. Adiabaticity in First-Principles Molecular Dynamics. *Phys. Rev. B* **1992**, *45*, 9413-9416.

(21) Pietrucci, F.; Andreoni, W. Fate of a Graphene Flake: A New Route toward Fullerenes Disclosed with Ab Initio Simulations. *J. Chem. Theory Comput.* **2014**, *10*, 913-917.

(22) Muñoz-Santiburcio, D.; Marx, D. On the Complex Structural Diffusion of Proton Holes in Nanoconfined Alkaline Solutions within Slit Pores. *Nat. Comm.* **2016**, *7*, 12625.

(23) Tabacchi, G.; Fois, E.; Calzaferri, G. Structure of Nanochannel Entrances in Stopcock-Functionalized Zeolite L Composites. *Angew. Chem. Int. Ed.* **2015**, *54*, 11112-11116.

(24) Koizumi, K.; Nobusada, K.; Boero, M. An Atomic-Level Insight Into the Basic Mechanism Responsible for the Enhancement of the Catalytic Oxidation of Carbon Monoxide on a Cu/CeO_2 Surface. *Phys. Chem. Chem. Phys.* **2017**, *19*, 3498-3505.

(25) Kraus, P.; Frank, I. On the Dynamics of H_2 Adsorption on the Pt(111) Surface. *Int. J. Quantum Chem.* **2017**, *117*, e25407.

(26) Capano, G.; Penfold, T. J.; Chergui, M.; Tavernelli, I. Photophysics of a Copper Phenanthroline Elucidated byTrajectory and Wavepacket-Based Quantum Dynamics: a Synergetic Approach. *Phys. Chem. Chem. Phys.* **2017**, *19*, 19590-19600.